ISSN: 3007-9640 DOI: https://doi.org/10.70114/acmsr.2026.6.1.P77

A Joint Time-Frequency Scaling Algorithm for Squint SAR Imaging

Liang Ni [1, a] *, Chengshan Yang [1, b], Jinqiang Zhang [1, c] and Yujie Liang [2, d]

[1] Shanghai Radio Equipment Research Institute, Shanghai 201109, China;

[2] School of Optoelectronic Engineering, Xidian University, Xi'an 710071, Shannxi, China.

[a] 176167384@qq.com, [b] 215823001@qq.com, [c] jqzhangemail@163.com, [d] liangyujie@xidian.edu.cn

Abstract. Squint radar imaging is an important working mode for synthetic aperture radar (SAR). To facilitate the accumulation of azimuth energy, range walk correction is commonly applied to straighten the envelopes of the scattering points. However, this process violates the principle of translation invariance, causing azimuth spatial-variant effects in range migrations and Doppler coefficients. Consequently, conventional imaging methods struggle to achieve effective and uniform focusing across the entire scene. To address this issue, this paper proposes a joint time-frequency scaling algorithm for squint SAR imaging. First, a keystone transform is employed to correct the spatial-variant range migration, thereby concentrating the energy of scattering points within a single range-sampling unit. Subsequently, variable scaling functions are introduced in both the time and frequency domains to compensate for the spatial variation of Doppler coefficients with azimuth position, effectively improving the azimuth focusing depth and achieving precise focusing of the entire scene. Experimental results validate the effectiveness of the proposed method.

Keywords: synthetic aperture radar (SAR); squint SAR imaging; range cell migration (RCM); scaling processing.

1. Introduction

Synthetic Aperture Radar (SAR) has become an indispensable core remote sensing tool in Earth observation because of its unique advantages of all-day, all-weather, long-distance, and high-resolution imaging [1], [2]. With the continuous deepening of application requirements, the traditional side-looking mode is no longer able to satisfy the requirements of continuous monitoring, rapid response, and complex terrain detection in specific areas, owing to its fixed observation direction and insufficient flexibility. Against this backdrop, squint SAR imaging technology has emerged, which actively steers the radar beam point in the forward or backward squint direction, achieving early observation and tracking of the forward or backward area of the flight platform trajectory [3], [4]. This mode not only significantly expands the visibility and mission flexibility of the SAR system, but also provides valuable maneuver and decision-making time for the continuous monitoring of key areas, moving target indication, and disaster emergency response, thus becoming an important direction for SAR technology development [5], [6].

However, the development of the squint mode, especially the application of high-squint SAR imaging, has brought new challenges, such as severe range cell migration (RCM) and complex two-dimensional coupling, rendering traditional imaging algorithms unsuitable. To address this issue, [7] proposes an improved SPECAN algorithm to address the consistent pixel spacing and practical processing requirements; however, the model is simple and difficult to apply to complex situations. [8] adopts the strategy of phase multiplication for envelope compensation in the two-dimensional frequency domain, but it cannot solve the RCM problem of the entire scene. Considering the spatial variation of the Doppler coefficients, [9] proposes an NCS method that partially addresses the issue of the Doppler frequency modulation (FM) rate. However, in the high-squint mode, defocusing still occurs at the edge position. [10] proposes an ENCS method; however, its application requires a large amount of padding with zeros to expand the support area, resulting in an enormous computational load that cannot satisfy practical requirements.

To solve the problem of squint SAR imaging, this paper proposes a joint time-frequency scaling (JTFS) algorithm. After performing uniform envelope compensation through range walk correction,

ISSN: 3007-9640 DOI: https://doi.org/10.70114/acmsr.2026.6.1.P77
a specific analysis is conducted on the remaining RCM. On this basis, a keystone transform (KT) is employed to correct the remaining migration components, enabling the scattering points' envelope to cluster within a single range-sampling unit. Next, to address the spatial variation of Doppler coefficients, scaling processing is applied in both the time and frequency domains to compensate for the azimuth variability components of Doppler FM rate and cubic FM rate, thereby achieving consistent focusing in the azimuth dimension. Finally, the effectiveness of the proposed method was verified through a simulation experiment.

2. Squint SAR Imaging

2.1 Geometric Model

Without loss of generality, a diving SAR imaging geometric model is established as shown in Fig. 1. The radar platform dives along the blue straight line with a speed of v and an elevation angle α. The antenna beam points towards the ground, forming a beam footprint indicated by the green ellipse.

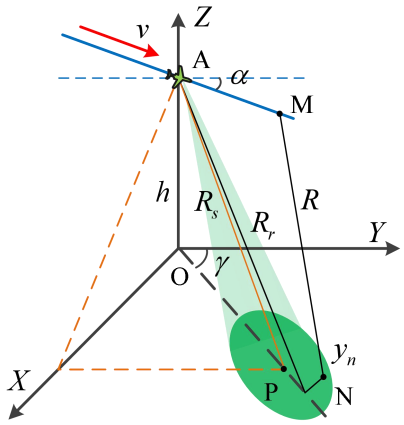


Fig. 1 Geometric model of squint SAR imaging

We use t_m to represent the azimuth slow time. Assuming that at the middle moment of slow time, the radar moves to point A directly above the origin, with a platform height of h. At any moment, the radar's position M can be represented as a function of azimuth time.

$$\mathrm{M}\left(x_M, y_M, z_M\right) = \left(0, vt_m \cos\alpha, vt_m \sin\alpha + h\right) \tag{1}$$

Point P is the intersection point between the beam centerline and the ground, OP is the projection of the beam centerline AP on the ground, $R_s = |\mathrm{AP}|$ represents the radar reference range, and γ represents the azimuth angle. Assuming point N is an arbitrary point within the beam footprint, represented by y_n for the vertical distance to OP and R_r for the corresponding slant range. Any point within the beam footprint can be uniquely determined by these two variables.

$$\mathrm{N}\left(x_N, y_N, z_N\right) = \left(\sqrt{R_r^2 - h^2}\sin\gamma + y_n\cos\gamma, -\sqrt{R_r^2 - h^2}\cos\gamma + y_n\sin\gamma, 0\right) \tag{2}$$

Therefore, the instantaneous slant range history can be expressed as $R\left(t_m; R_r, y_n\right) = |\mathrm{MN}|$.

By performing a Taylor series expansion with respect to azimuth time [11], we can obtain:

$$R\left(t_m; R_r, y_n\right) = \sum_{i=0}^{\infty} k_i\left(R_r, y_n\right) t_m^i \tag{3}$$

Where k_i represents the Taylor expansion coefficient, which usually satisfies the accuracy requirements up to the fourth order.

ISSN: 3007-9640 DOI: https://doi.org/10.70114/acmsr.2026.6.1.P77

The pulse compression processing of linear frequency modulation (LFM) signals can effectively improve the range resolution, which will not be repeated here. Perform range dimension FFT after pulse compression to obtain the signal in the range frequency domain.

$$Ss\left(f_r,t_m\right)=A_0W_r\left(t_r\right)w_a\left(t_m\right)\exp\left\{-j\frac{4\pi\left(f_c+f_r\right)R\left(t_m\right)}{c}\right\} \tag{4}$$

Among them, A_0 represents the signal amplitude, which has no impact and is often ignored in SAR imaging. $W_r\left(\cdot\right)$ and $w_a\left(\cdot\right)$ represent the range and azimuth envelopes, f_c represents the carrier frequency, f_r represents the range frequency, and c represents the speed of light.

2.2 RCM correction

In squint SAR imaging, there is a non-negligible migration effect in the slant range history of scattering points, and the energy within the echoes will also display an inclined distribution pattern. Therefore, range walk correction must be performed first, and unified RCM correction should be carried out through phase compensation [12].

$$H_{RWC}\left(f_r,t_m\right)=\exp\left\{j\frac{4\pi\left(f_c+f_r\right)}{c}k_{10}t_m\right\} \tag{5}$$

Where k_{10} represents the first-order expansion coefficient of the slant range process

Actually, (5) only eliminates the linear reference component of RCM. Residual components can still cause the energy distribution of points at the scene edge to span multiple range-sampling units. To address this issue, this paper introduces the KT to achieve residual RCM correction. By defining a virtual slow time variable, the keystone transform stretches and compresses the radar echo along the slow time dimension in the range frequency domain, thereby compensating for the envelopes displacement away from the scene center, which can be expressed as:

$$t_m'=\frac{f_c+f_r}{f_c}t_m \tag{6}$$

where t_m' is virtual azimuth slow time defined in KT.

Substituting (6) into the signal after range walk correction, we can obtain:

$$Ss'\left(f_r,t_m'\right)=W_r\left(f_r\right)w_a\left(t_m'\right)\cdot\exp\left\{-j\phi_{KT}\right\} \tag{7}$$

Where:

$$\phi_{KT}=\frac{4\pi\left(f_c+f_r\right)}{c}k_0+\frac{4\pi f_c}{c}\left(k_1-k_{10}\right)t_m'+\frac{4\pi\left(f_c+f_r\right)}{c}\left[\sum_{i=2}^{4}k_i\left(\frac{f_c}{f_c+f_r}t_m'\right)^i\right] \tag{8}$$

It is evident that there is no coupling between $\left(k_1-k_{10}\right)t_m'$ and range frequency f_r, which means the linear RCM is corrected accurately. By ignoring high-order spatial variations with minimal impact, accurate RCM correction can be achieved over the entire scene.

For simplicity, replace t_m' with t_m and perform range IFFT on the signal to obtain the range dimension focusing result:

$$ss\left(t_r,t_m\right)=\sin c\left\{B_r\left[t_r-\frac{2R_0}{c}\right]\right\}\cdot w_a\left(t_m\right)\cdot\exp\left\{-j\frac{4\pi}{\lambda}\left(\sum_{i=0}^{4}k_i{t_m}^i\right)\right\} \tag{9}$$

At this point, the range and azimuth dimensions are no longer coupled with each other, and the scattering point's energy will be concentrated within a single range-sampling unit in the time domain.

ISSN: 3007-9640 DOI: https://doi.org/10.70114/acmsr.2026.6.1.P77

2.3 Joint time-frequency scaling

The spatial variation of Doppler phase will seriously limit the azimuth focus depth and affect the imaging quality. Therefore, it is necessary to adopt the JTFS to eliminate the spatial variation of Doppler phase. We expand the azimuth phase with respect to the azimuth position y_n by Taylor series.

$$\varphi(t_m;y_n)=2\pi\left(b_0(y_n)+\sum_{i=1}^{4}\left(\sum_{j=0}^{4-i}b_{ij}{t_m}^i{y_n}^j\right)\right) \tag{10}$$

where $b_{ij}=-2k_{ij}/\lambda$.

Among all spatial variant components, $b_{21}{t_m}^2y_n$, the linear spatial variant component of FM rate, has the most significant impact on azimuth focusing. Therefore, the linear spatial variant component of FM rate is the primary consideration in the azimuth processing. The traditional NCS algorithm introduced a third-order scaling term in the Doppler domain [9], which can achieve accurate compensation for this term.

Then, the quadratic spatial variation of FM rate $b_{22}{t_m}^2{y_n}^2$ and the linear spatial variation of cubic FM rate $b_{31}{t_m}^3y_n$ will also affect the azimuth focusing. [4] introduces a fourth-order scaling term based on the traditional NCS algorithm. Even so, it can only compensate for one of those two terms and need to make a choice between them. In order to accurately compensate for those simultaneously, we can adopt new scaling terms both in the azimuth time domain and Doppler domain, respectively, and introduce a second-order scaling term in the Doppler domain to change the stationary phase point in IFFT. In this way, the simultaneous compensation of those spatial variant terms could be realized, further improving the focusing accuracy and imaging quality.

According to the previous discussion, after compensating for the spatial invariant phase component, the time scaling function is introduced in the azimuth time domain:

$$H_{time}(t_m)=\exp\left\{j2\pi\left(p_3{t_m}^3+p_4{t_m}^4\right)\right\} \tag{11}$$

Where p_i represents the scaling coefficient in the time domain, and its specific expression could be obtained through subsequent processing. By performing the azimuth FFT, the frequency scaling function is introduced in the Doppler domain:

$$H_{frequency}(f_a)=\exp\left\{j2\pi\left(q_2{f_a}^2+q_3{f_a}^3+q_4{f_a}^4\right)\right\} \tag{12}$$

where q_i represents the scaling coefficient in the Doppler domain, and its specific expression could be obtained through subsequent processing, too.

The azimuth phase after azimuth IFFT can expanded by Taylor series concerning the azimuth time and azimuth position. We use $\mu=1-4b_{20}q_2$ to represent the azimuth scaling factor, and the result could be shown in the follow.

$$\begin{aligned}\varphi'(t_m;y_n)\approx{}&A(p_3,p_4,q_2,q_3,q_4;t_m)+B(q_2)\left(\frac{t_m}{\mu}\right)y_n+C(p_3,q_2,q_3)\left(\frac{t_m}{\mu}\right){y_n}^2+D(p_3,q_2,q_3)\left(\frac{t_m}{\mu}\right)^2y_n\\&+E(p_3,p_4,q_2,q_3,q_4)\left(\frac{t_m}{\mu}\right)^2{y_n}^2+F(p_3,p_4,q_2,q_3,q_4)\left(\frac{t_m}{\mu}\right)^3y_n+G(p_3,p_4,q_2,q_3,q_4;y_n)\end{aligned} \tag{13}$$

In (14), the first term represents the spatial invariant phase component arisen in the JTFS processing, which can be eliminated by the subsequent azimuth Deramp processing. The second and third terms are the first-order term of azimuth slow time, representing the scattering point's theoretical position and distortion position caused by SAR imaging. The fourth and fifth terms are the second-order term of azimuth slow time, representing the linear and quadratic spatial variation

ISSN: 3007-9640 DOI: https://doi.org/10.70114/acmsr.2026.6.1.P77
of Doppler FM rate changing with azimuth position. The sixth term is the third-order term of azimuth slow time, which means the linear spatial variation of cubic FM rate. The last term represents the resident phase that is independent of azimuth focusing and can be ignored.

As analyzed previously, the equations with all scaling coefficient as unknown coefficient can be written as:

$$\begin{cases} C\left(p_3,q_2,q_3\right)=0 \\ D\left(p_3,q_2,q_3\right)=0 \\ E\left(p_3,p_4,q_2,q_3,q_4\right)=0 \\ F\left(p_3,p_4,q_2,q_3,q_4\right)=0 \end{cases} \tag{14}$$

And we can obtain all the coefficients by solving the equations.

By substituting the scaling coefficients into the JTFS processing, the accurate compensation of the spatial variant Doppler phase can be realized [4]. At the same time, we can eliminate the spatial invariant phase and perform azimuth FFT to obtain the focusing result in the Range-Doppler domain.

$$ss\left(t_r,f_a\right)=\sin c\left\{B_r\left[t_r-\frac{2R_0}{c}\right]\right\}\cdot\sin c\left\{T_a\left(f_a-\frac{b_{11}}{\mu}y_n\right)\right\} \tag{15}$$

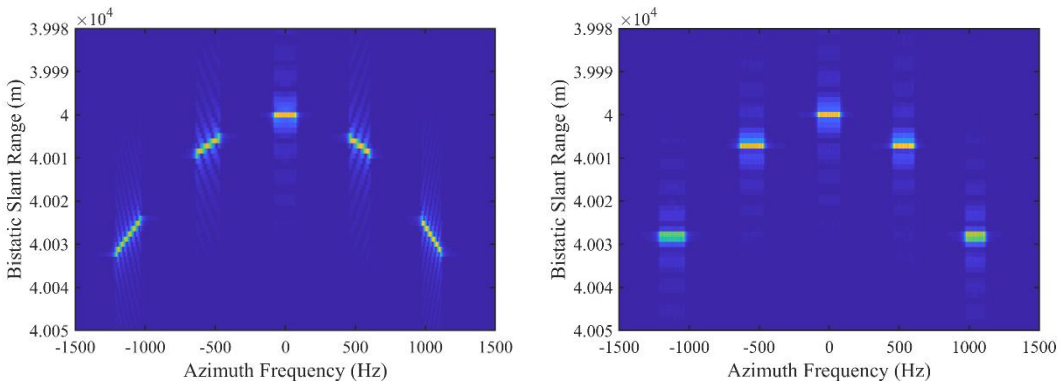
Where $\left(b_{11}y_n/\mu\right)$ represents the focus position in the Doppler domain.

3. Simulation Experiments

To verify the performance of the proposed algorithm, simulation experiments are carried out in this section. We divide the simulation experiments into two parts. The first part explains the advantages of KT processing in RCM correction, and the second part demonstrates the effectiveness of the proposed JTFS method. Simulation parameters are listed in Table I. Assume the swath of the imaging area is 3km in the range and azimuth dimensions, in which a 5×5 point array is uniformly arranged to imitate scattering points at different positions

Table 1 Simulation Parameters

Parameters	Value	Parameters	Value
Reference Slant Range	40km	Pulse Width	10μs
Azimuth Angle	30°	Signal Bandwidth	100MHz
Grazing Angle	15°	Sampling Frequency	120MHz
Velocity	(500,100,-200)m/s	Pulse Repetition Frequency	5000Hz



(a) Before KT (b) After KT

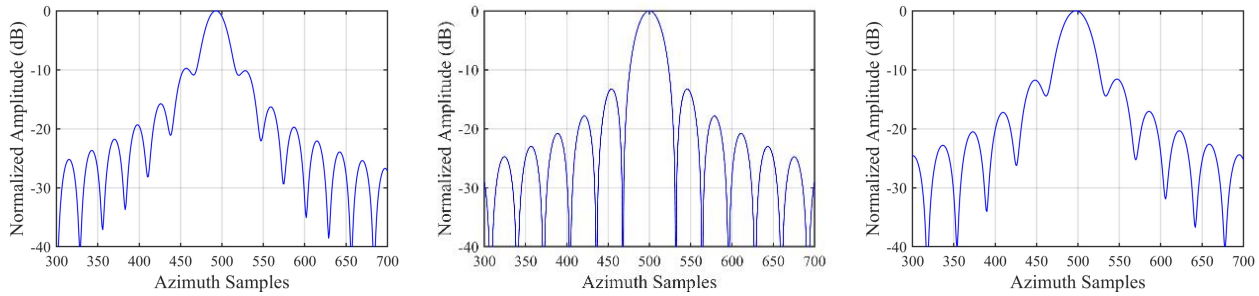
ISSN: 3007-9640 DOI: https://doi.org/10.70114/acmsr.2026.6.1.P77

Fig. 2 RCM correction results

Part I: We take the scattering points in the central row to examine the effectiveness of RCM correction. The envelopes before and after KT processing are shown in Fig. 2. Owing to the inability of range walk correction to handle the spatial variation in RCM, the residual RCM component in subfigure (a) increases with the displacement of scattering points, and the edge positions can span up to 8 range-sampling units. Directly processing the azimuth dimension will result in severe leakage of scattering points' energy. After correcting the residual RCM through KT processing, the envelope changes shown in Fig. 2(b) are all moved to a single range-sampling unit, where range and azimuth are completely decoupled, providing great convenience for subsequent azimuth processing.

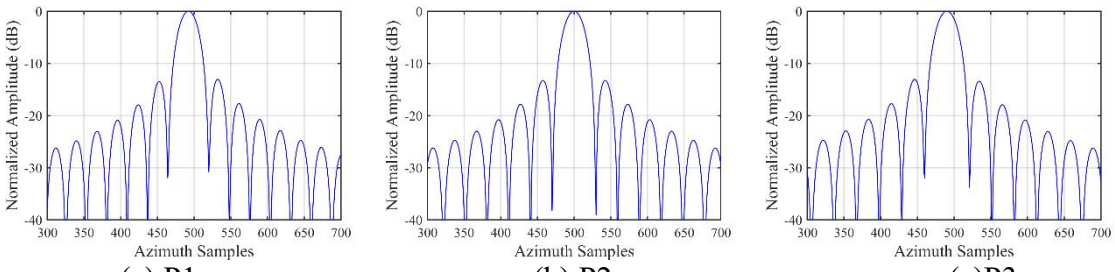
Part II: After deeply decoupling in the range and azimuth dimensions, we select the left edge point of the nearest range unit as P1 and the right point of the farthest range unit as P3 to conduct a specific analysis of the azimuth focusing results, and use the center point as a reference marked P2. Due to insufficient consideration of the spatial variation of Doppler coefficients in the traditional method [9], there is still a residual error at the edge point that causes widening of the main-lobe and elevation of the side-lobes. This makes it impossible for azimuth profiles of the edge points to present a standard sinc shape like the center point, as shown in Fig. 3.

In comparison, the azimuth impulse response profile of the proposed method is shown in Fig. 4. Since the linear and quadratic spatial variation of FM rate and the linear spatial variation of cubic FM rate have been eliminated, the residual phase error is small enough not to affect the azimuth focusing. So the azimuth profile is basically similar to an ideal sinc function. Fig 5 shows the contour plot, demonstrating that the main lobe and side lobe are separated clearly, presenting an ideal “cross”.



(a) P1 (b) P2 (c)P3

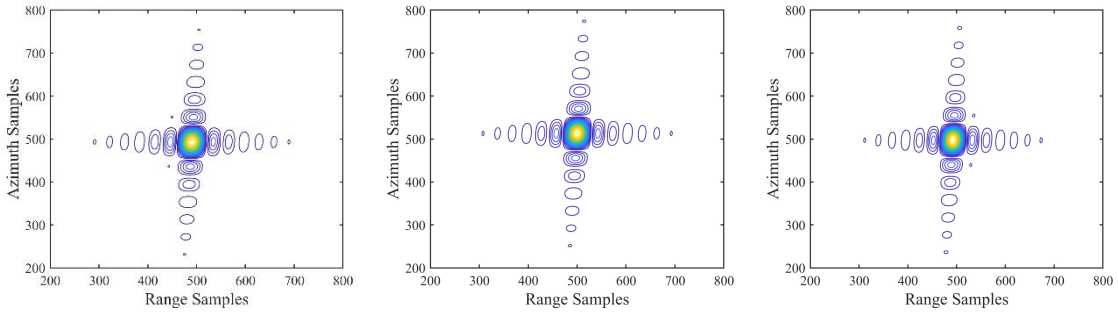
Fig. 3 Azimuth profiles of three points obtained by the traditional method



(a) P1 (b) P2 (c)P3

Fig. 4 Azimuth profiles of three points obtained by the proposed method

ISSN: 3007-9640 DOI: https://doi.org/10.70114/acmsr.2026.6.1.P77



(a) P1 (b) P2 (c)P3

Fig. 5 Contour plots of three points obtained by the proposed method

4. Summary

In this paper, a JTFS algorithm is proposed for squint SAR imaging. We adopt the keystone transform to correct the spatial-variant RCM, so that the energy of scattering points can be concentrated in a single sampling unit. Subsequently, the time and frequency scaling functions are introduced to accurately compensate for the spatial variation of the Doppler FM rate and cubic FM rate that affect the azimuth focus processing. and finally achieve accurate focusing in the range Doppler domain. The proposed algorithm can be applied to squint SAR imaging with a complex configuration, and can be further applied to the fields of reconnaissance and detection.

References

[1] Cumming Ian G, Wong Frank H. Digital Processing of Synthetic Aperture Radar Data: Algorithms and Implementation; Artech House: Norwood, MA, USA, 2005, pp. 3-17.

[2] Moreira Alberto, Prats-Iraola Pau, Younis Marwan, et al. A tutorial on synthetic aperture radar. IEEE Geoscience and Remote Sensing Magazine, 2013, 1, 6-43.

[3] Song Yufan, Zhang Jingjing, Jin Shuang, et al. Frequency-Scaling-Based Spaceborne Squint SAR Sparse Imaging, vol. 2022, 15, 8064-8073.

[4] Liang Yi, Li Zhenyu, Zeng Letian, et al. A High-Order Phase Correction Approach for Focusing HS-SAR Small-Aperture Data of High-Speed Moving Platforms, IEEE Journal of Selected Topics in Applied Earth Observations and Remote Sensing, 2015, 8(9): 4551-4561.

[5] Yang Jiefang, Zhang Yunhua, Kang Xueyan, et al. A Doppler Ambiguity Tolerated Algorithm for Airborne SAR Ground Moving Target Imaging and Motion Parameters Estimation, IEEE Geoscience and Remote Sensing Letters, 2015, 12(12): 2398-2402.

[6] Luo Yunhua, Song Hongjun, Wang Robert, et al. Arc FMCW SAR and Applications in Ground Monitoring, IEEE Transactions on Geoscience and Remote Sensing, 2014, 52(9): 5989-5998.

[7] Fang Lili, Wang Xuetian, Wang Yifeng. A Modified SPECAN Algorithm for Synthetic Aperture Radar Imaging, 2010 International Conference on Measuring Technology and Mechatronics Automation, 2010.

[8] Dang Yanfeng, Liang Yi, Bie Bowen, et al. A Range Perturbation Approach for Correcting Spatially Variant Range Envelope in Diving Highly Squinted SAR with Nonlinear Trajectory, IEEE Geoscience and Remote Sensing Letters, 2018, 15(6): 858-862.

[9] Li Zhenyu, Liang Yi, Xing Mengdao, et al. A sub-aperture imaging algorithm for highly squinted SAR based on frequency phase correction. 2015 IEEE 5th Asia-Pacific Conference on Synthetic Aperture Radar, 2015.

[10] Wang Zhigui; Liu Mei; Ai Gengting, et al. Focusing of Bistatic SAR with Curved Trajectory Based on Extended Azimuth Nonlinear Chirp Scaling, IEEE Transactions on Geoscience and Remote Sensing, 2020, 58(6): 4160-4179.

ISSN: 3007-9640 DOI: https://doi.org/10.70114/acmsr.2026.6.1.P77
[11] An Hongyang, Wu Junjie, Sun Zhichao, et al. A Two-Step Nonlinear Chirp Scaling Method for Multichannel GEO Spaceborne–Airborne Bistatic SAR Spectrum Reconstructing and Focusing, IEEE Transactions on Geoscience and Remote Sensing, 2019, 57(6): 3713-3728.

[12] Zhang Duo, Wu Fuwei, Qiu Guangfeng. An Improved Airborne High Squint PFA Imaging Algorithm Combined with Linear Range Walk Correction. 2024 9th International Conference on Signal and Image Processing, 2024.